Using AVHRR to correct for clouds in IASI observations.

Andrew De seja-Martin.
UNIQ+ Research Internship
Supervisor: Dr Anu Dudhia
AOPP, Department of Physics, University of Oxford.
(Dated: September 6, 2026)

Investigated was the potential to use the Infrared Atmospheric Sounding Interferometer (IASI) and the Advanced Very High Resolution Radiometer (AVHRR) onboard the MetOp-C satellite in analysing cloudy scenes and their practical application in compensating for cloud effects in retrievals of atmospheric composition. The percentage of AVHRR pixels that represented the most cold region found within an IASI footprint was found not to agree with the IASI cloud percentage. The affect of the incorporation of auxiliary information, provided by AVHRR, was considered on atmospheric methane retrievals over the ocean and approaches on improving the treatment of clouds was analysed. The utilisation of AVHRR data was found to mixed affects, initially increasing the disparity between the mean methane values for clear and cloudy pixels but later improvements were made. Notwithstanding modest improvements the retrieval process still faced uncertainties and trade off's. It was found not entirely possible to achieve a fully satisfactory result for methane retrievals using AVHRR data alone.

I. INTRODUCTION

The earliest examples of infrared remote sensing dates back to the mid 1960s with the Nimbus series of satellites. They were experimental weather and climate monitoring systems [1] which paved the way for satellites such as the Meteorological Operational (MetOp) satellites decades later; they are immensely important for observations of trace elements, atmospheric temperature and water vapour measurements for weather forecasting. The MetOp-C satellite launched in 2018 provides the basis for this report. The MetOp satellite has a polar orbit with an altitude of just over 800 kilometres above sea level [2]. This particular orbit configuration allows the ability to cover most of the Earths surface, twice in a 24 hour period. Onboard the MetOp-C satellite is the Infrared Atmospheric Sounding Interferometer (IASI) instrument which is fine-tuned to measure infrared radiation emitted from the Earth. IASI has a spatial resolution of 12 kilometres meaning each footprint has a comparatively coarse field of view, one which may contain many geographical, oceanic and atmospheric features within it including, crucially, clouds. IASI does however provide high spectral resolution of approximately 0.25 cm^{-1}. The high spectral detail provided from IASI can ostensibly deblend complex infrared spectra, allowing retrieval algorithms to isolate weak absorption signatures from that of trace gases (such as methane, carbon monoxide, and nitrous oxide) from that of more prominent background features like that from water vapour and carbon dioxide.

As the satellite orbits the Earth, IASI scans a position with 4 individual footprints in a 2 by 2 pattern of 50 kilometres squared similarly to that shown in figure 1, measuring the radiance received in each one. IASI measures the received spectral radiance at the top of the atmosphere. Features such as temperature profiles, trace element concentrations and cloud characteristics are not measured directly. Instead they are interpreted from the observed spectrum using radiative transfer modelling making a forward model prediction. Any cloud within an IASI footprint obscures the warmer surface below, reducing the overall radiance reaching the satellite due to the lower temperatures at higher altitudes. The amount of radiance received is also affected by the type of cloud (water or ice), as well as the optical thickness of cloud, though this was not considered within this report. The standard practice is to discard any IASI footprint that contains any cloud contamination, this results in a lot of IASI cloud contaminated spectra being lost. Proper determination of the percentage of cloud within the IASI footprint and cloud top temperatures would be necessary in order to adjust retrieval algorithms to produces accurate results for element compositions under cloudy conditions. For each IASI footprint various flags can be assigned to categorize scenes based on, for example cloud coverage (cld) and whether the pixel is over land (lnd). By leveraging these flags one can isolate specific conditions such as separating clear sky scenes from cloudy ones. An illustration on how the presence of clouds affects the radiance is shown in figure 2.

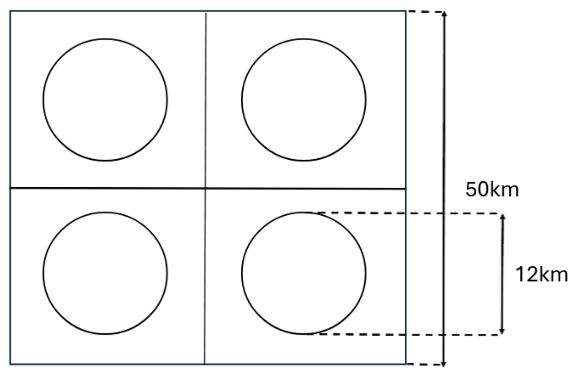

FIG. 1. Schematic representation of the IASI footprint structure showing the 2 × 2 pattern. Each circular footprint has a field of view of approximately 12 km.

Also onboard the MetOp-C satellite is the Advanced Very High Resolution Radiometer (AVHRR), which acts as a complement to IASI. While IASI provides high spectral detail, AVHRR provides high spatial detail with a pixel field of view of around 1 kilometre. Each IASI footprint contains multiple higher resolu-

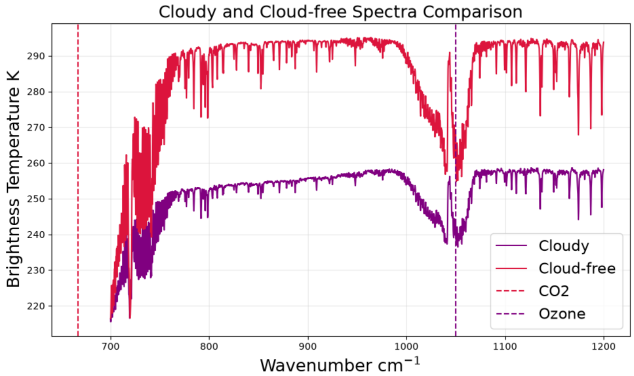

FIG. 2. Effect of cloud coverage on the received radiance measurements of IASI. The effect of cloud reduces the brightness temperature (see section II) from around 290 K to 250 K, due to the emission being primarily from the cloud tops, which is at a colder temperature than the ground surface. The dashed lines represent the centre locations of the absorption features for ozone and carbon dioxide. The edge of the carbon dioxide band can be seen from 700-800 cm^{-1}.

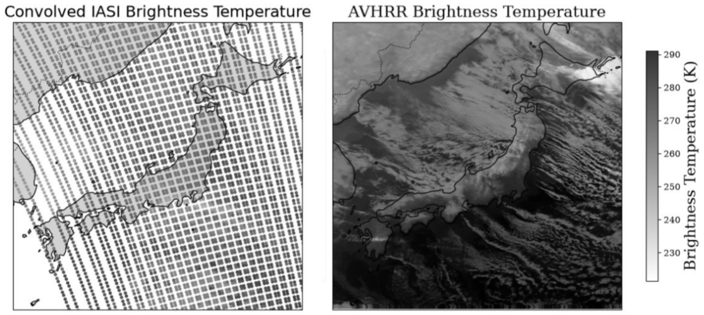

FIG. 3. Comparison of satellite brightness temperature swaths by IASI (left) and AVHRR (right). The fine-scale resolution of AVHRR reveals detailed structures such as the horizontal convective rolls (cloud streets) of the South-East coast of Japan, whereas the IASI footprints shows a smoothing out of the region heterogeneities. The IASI spectra have been convolved with the AVHRR spectral response function.

tion AVHRR pixels (as represented in figure 3), each with an associated radiance value, AVHRR can group together pixels with a similar radiance into clusters as well as allocate the mean radiance (R_{av}) and its fractional coverage (Pct) within the larger IASI footprint. The number of clusters range from 1 to 7 and can be filtered with the (Ncl) flag. IASI measures radiance across a continuous high-resolution spectrum whereas, AVHRR measures radiance in many distinct spectral channels spanning the visible and thermal infrared part of the electromagnetic spectrum. The spectral range of 700-1200 cm^{-1} is a region acting as a spectral window (where atmospheric gases don't strongly absorb or scatter radiation) [3]. The top of the atmosphere responds proportionally to changes in cloud coverage in the region and was the focus of this report. Hence, only AVHRRs Channel 4 (10.3–11.3μm) and Channel 5 (11.5–12.5μm) were considered.

The retrieval process, discussed later, relies on optimal estimation and prediction, which iteratively minimize the difference between the observed radiance and a forward model prediction based on initial atmospheric parameters.

II. INSTRUMENT RESOLUTION AND BRIGHTNESS TEMPERATURE

IASI and AVHRR measure spectral radiance rather than directly measuring the temperature. To better interpret the measurements, it is customary to routinely convert the radiance values into brightness temperature T_b, which is defined as the temperature a black body would need to be in order to emit the observed radiance at a given wavelength (see appendix for equations used to convert from radiance to brightness temperature).

Figure 3 shows the convolved (see section III) IASI spectra and the AVHRR channel 4 brightness temperature swaths over Japan which highlights the difference in the spacial resolution of both instruments. Whereas the coarse IASI footprint provides a smooth, generalised overview of a regional areas radiance, the higher resolution AVHRR pixels can resolve fine scale metrological features.

III. SPECTRAL RESPONSE VALIDATION

Prior to looking at retrievals, it was important to provide an in depth analysis on the information provided by both the IASI and AVHRR instruments to determine whether they imply consistent physical states for a given footprint. Due to the fact IASI produces a continuous high resolution spectra while AVHRR measures broad bands with varying sensitivity, direct comparison was not possible. Instead, it was necessary to weight the IASI spectrum with the Spectral Response Function ($\Psi(\nu)$) for each specific channel, simulating the measurement AVHRR would record if it observed the IASI spectrum. The AVHRR Spectral Response Function describes how sensitive each channel is to radiation across different wavelengths. Rather than measuring radiance at a single wavelength, each AVHRR channel detects radiation over a finite spectral range, with varying sensitivity across that range. Equation 1 defines the mathematical relation used to calculate the convolved IASI radiance R_c,

$$R_c = \int \Phi(\nu) R(\nu)\, \mathrm{d}\nu \simeq \sum_i \Phi(\nu_i) R_I(\nu_i) \qquad (1)$$

where $\Phi(\nu)$ is the normalised signal response function, $R_I(\nu_i)$ is the IASI radiance at wave number ν_i. We would expect that the convolved radiance would be consistent with the AVHRR channel 4 and 5 values.

For a randomly selected footprint, a strong baseline agreement between the two instruments was demonstrated. The percentage differences between the AVHRR channel 4 and 5 values and the corresponding convolved IASI values were 0.38 and 0.40 percent respectively. The small percentage differences indicate that both instruments could be radiometrically compatible. To test this consistency more rigorously across a broader dataset, the predicted average AVHRR radiance was directly compared with the convolved IASI spectrum for each footprint. The analysis was restricted to ocean scenes ($lnd == 0.0$) to avoid complex land emissivity effects. The predicted average AVHRR radiance R_{AVHRR} was calculated using Equation 2,

$$R_{AVHRR} = \frac{\Sigma(R_{\mathrm{av}} \times pct)}{\Sigma pct} \tag{2}$$

where R_{av} is the average radiance associated with each cluster and pct is the associated cluster fraction size.

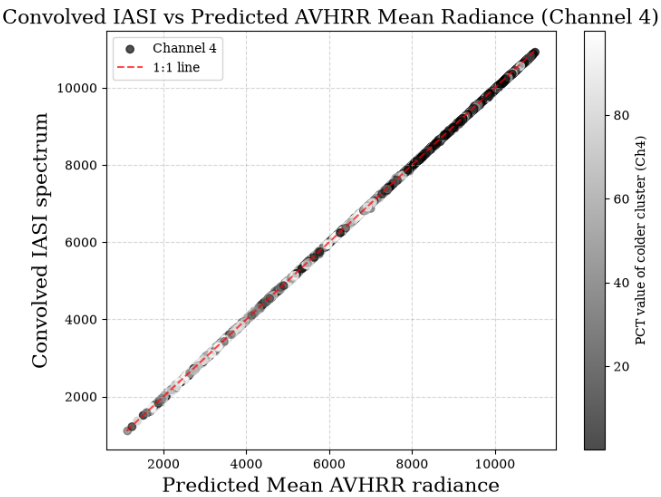

FIG. 4. Figure showing the convolved IASI spectrum as a function of the predicted mean AVHRR radiance for channel 4, the dotted line represents the expected 1 to 1 relation.

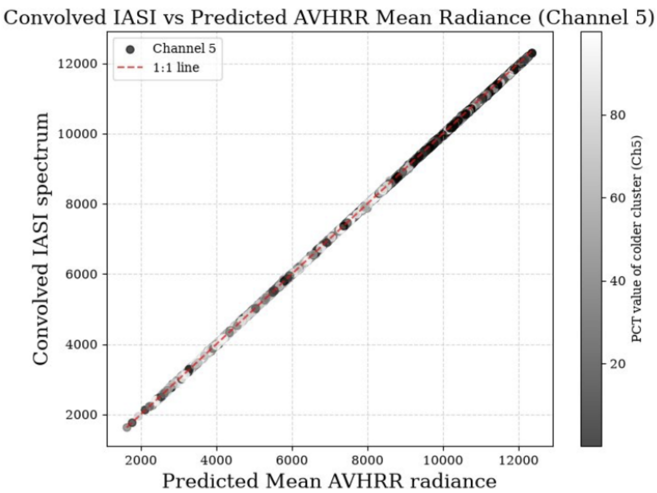

FIG. 5. Figure showing the convolved IASI spectrum as a function of the predicted mean AVHRR radiance for channel 5, the dotted line represents the expected 1 to 1 relation.

The results shown in figures 4 and 5 shown an unimpeachable linear relation, matching the 1-to-1 expectation which further verifies that both instruments are radiometrically compatible. Notwithstanding that fact figures 4 and 5 are examples of two cluster cases, identical results were found for all cluster types, reasonably validating the result. For a partially cloudy two cluster scene, it can be said that the warmest AVHRR cluster, that is the cluster which contains the pixels with the highest radiance values, could represent the cloud free surface or ocean in the case of this report. Conversely, the colder cluster would then serve as a representation for the cloud surface. Accurately identifying the ground surface and being able to calculate the brightness temperature would become extremely useful in evaluating the performance of the retrieval algorithm (see section V).

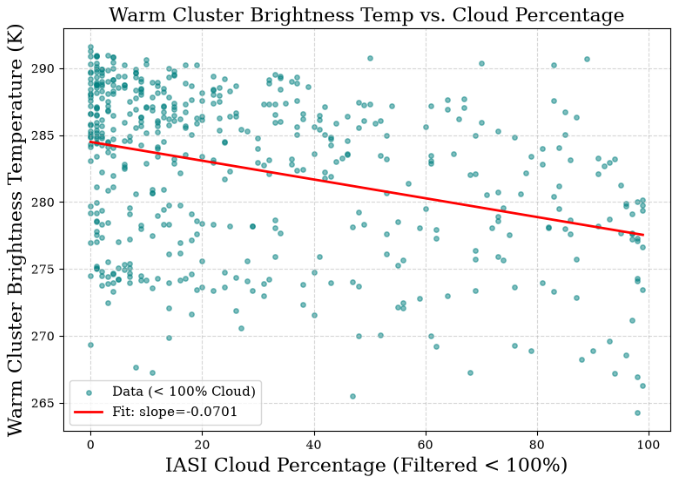

FIG. 6. Brightness temperature of the warmest cluster as a function of IASI cloud percentage, filtering out completely cloudy scenes. The linear fit has a slope of 0.07.

As shown in Figure 6, the temperature variation of the warm cluster is negligible across a vast amount of points, yielding a linear fit of 0.07. The brightness temperatures cluster closely around 270 to 290 K, which is consistent with a warm ocean surface (whereas clouds would exhibit significantly lower temperatures normally near 240 K). Consequently, we can be fairly confident that the warmest cluster within a partially cloudy IASI footprint serves as a reliable proxy for the clear sky ocean background. Although, it is worth acknowledging the fact a significant number of pixels show radiance values below 270 K which is most likely due to cloud contamination.

IV. IASI CLOUD PERCENTAGE ANALYSIS

The results shown in Figure 7 are very revealing indeed. The previous section showed that the two instruments are radiometrically compatible, so one would expect that they would agree on the percentage of cloud within an IASI footprint, that is to say there would exist a linear correlation between the fraction of AVHRR pixels within the colder cluster and the IASI cloud percentage. The IASI cloud percentage acts a value indicative of the amount of cloud that the IASI instrument suggests is within a particular scene. This is not the case and figure 6 indicated that the fraction of

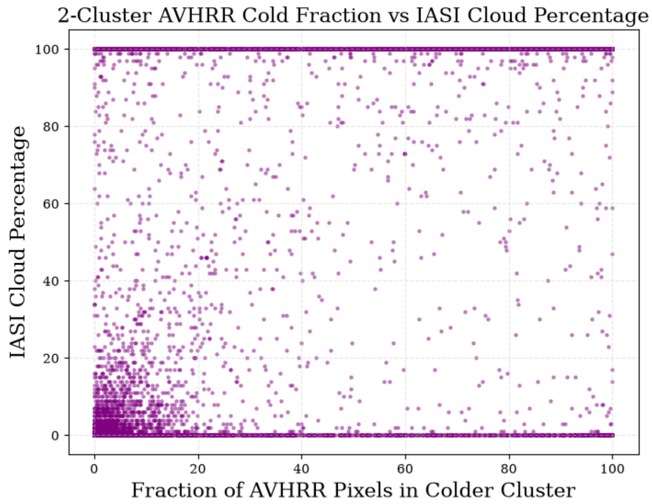

FIG. 7. Figure showing the IASI cloud percentage as a function of the percentage of AVHRR pixels within the colder cluster in a two cluster model.

AVHRR pixels falling into the cold cluster did not reliably correlate with the official IASI cloud percentage. This stark disagreement raises serious questions about the reliability of using a naive AVHRR cluster counting method to model clouds within an IASI footprint, that is attributing the fraction of pixels within the coldest AVHRR cluster to the cloud fraction. One potential reason for this scatter is that homogeneous scenes, where the two clusters have relatively similar radiances, might introduce difficulty in identifying an obvious cold cluster. To test this, homogeneous cases were filtered out by removing data points where the two cluster radiances were within 5 percent of each other. Furthermore, solar zenith angle (sza) flags were applied to separate day ($sza < 90°$) and night ($sza > 90°$) observations.

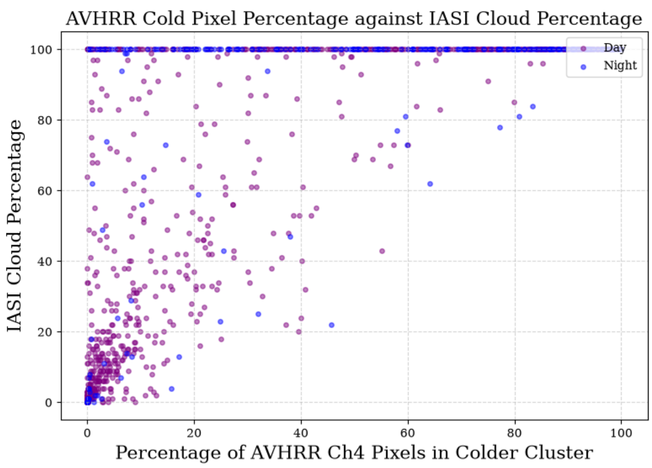

FIG. 8. Figure showing the IASI cloud percentage as a function of the percentage of AVHRR pixels within the colder cluster removing homogeneous scenes with day and night pixels highlighted.

We would expect a linear correlation between fraction of AVHRR pixels within the coldest cluster and the IASI cloud percentage, however, even after filtering out homogeneous scenes, Figure 7 shows that a simple AVHRR cold-cluster fraction systematically fails to track the physical IASI cloud percentage, often severely underestimating cloud cover. Additionally, the overlay of day and night pixels demonstrates that the solar zenith angle has no noticeable impact on this discrepancy, ruling out daytime thermal contrast artifacts as the root cause. The persistent mismatch suggested that a binary assumption, treating the cold cluster as cloud is perhaps overly simplistic. Sub footprint cloud fractions cannot be accurately gauged by raw pixel counting alone because AVHRR pixels are not simply cloud or cloud free but may often contain a blurred mix of the two. Because inaccurate cloud fractions introduce major errors into atmospheric trace gas retrievals. This outcome directly motivated pivoting the project to bypass pixel counting entirely and instead potentially integrating the insights found into the MORSE retrieval framework via building smarter mathematical constraints and refining how cloud temperatures are accounted for during methane column extractions.

V. METHANE RETRIEVAL

To evaluate the practical application of thorough advanced cloud treatment, the MORSE retrieval algorithm [4] used by the Earth Observation Data Group at the University of Oxford was executed on a small subset of 101 pixels off the coast of Japan. The region was selected due to it complex and variable cloud structure, providing a robust sample spanning the full 0-100 percent range of the IASI cloud percentage. The standard approach is to simply discard any IASI footprints that contain even a hint of cloud contamination, this leads to the loss of a lot of valuable spectra data. The objective was to assess how incorporating high resolution auxiliary AVHRR derived cloud properties, as opposed to coarse assumptions, affected retrieved methane column values, surface temperature and convergence, as well as data variance. Methane is a greenhouse gas that has short-term but potent effect on climate change [5]. Within the MORSE retrieval algorithm, accurately specifying the cloud top temperature and effective cloud cover fraction is vital for accurate retrieval. IASI footprints (12 km) could encapsulate heterogenous scenes and hence explains the premise for utilising AVHRR sub footprint (1 km) clusters to evaluate a clean delineation of the retrieval process. In the MORSE retrieval process the algorithm iteratively adjusts state parameters to minimise the difference between the forward model simulation and the actual satellite observation. The state parameter is function of local conditions such as pressure, temperature profile and surface emissivity. Chi-Squared (χ^2) acts as a statistical value representing, in essence, the effective performance of MORSE, where a lower χ^2 value indicates a closer match between the modelled spectra and the observed data.

To evaluate the impact of incorporating the AVHRR data, three distinct configurations of the MORSE retrieval algorithm were tested with varying approaches to cloud treatment.

- **Version 1:** Intended to order the individual AVHRR clusters within the larger IASI footprint by increasing average radiance (R_{av}, coldest first) and cumulatively summed until their combined cluster fraction (Pct) exceeded the IASI cloud percentage threshold. A weighted average of their respective radiances was then converted to a representative cloud brightness temperature.
- **Version 2:** Was designed to test whether small IASI cloud percentages inadvertently incorporated dominant ocean clusters which would ultimately skew the cloud temperatures, the version accumulated the clusters just before the IASI cloud percentage threshold was breached.
- **Version 3:** The AVHRR clusters were ordered in decreasing order (warmest first) and accumulated up to the clear percentage (100 − IASI cloud percentage). The remaining cold clusters were isolated to calculate a brightness temperature, and crucially, the IASI cloud percentage was then explicitly reassigned to match the exact combined AVHRR cold cluster fraction for internal consistency.

The performance of MORSE was evaluated by establishing a cloud-free baseline where atmospheric parameters are stable and well constrained [6]. Deviations in the methane column value and surface temperature relative to the clear sky baseline were then recorded across varying cloud fractions to isolate algorithmic uncertainty. Across all configurations, the cloud-free subset established a stable baseline mean methane concentration of 1.6107 ppmv with a minimal standard deviation of 0.0105, reflecting high precision and consistency under cloud-free conditions. The mean surface temperature for cloud free scenes was 285 K. However, for cloudy scenes, the introduction of explicit AVHRR cloud data and refined cluster weightings altered both the mean state and data scatter. The retrieved methane column values were plotted against the IASI cloud percentage, and the outputs with and without the introduction of AVHRR data were compared, this is represented by a CLD flag as can be seen in figure 9. In the standard unflagged configuration, cloudy retrievals yielded a mean methane value of 1.6306 ppmv (σ =0.0835), across all versions of MORSE considered, with only 1 failed retrieval. Utilizing the initial version 1 approach with the AVHRR cloud data, cloudy scenes yielded a mean methane value of 1.6849 ppmv with a standard deviation of 0.0695. The average surface temperature deviation from the clear scene was found to be -22.65 K. This configuration resulted in 23 failed retrievals out of the 101 point dataset, establishing an initial baseline for the trade-off between cloud flagging and convergence.

Hypothesized was the issue of edge case contamination, where a small IASI cloud percentage may inadvertently incorporate a dominant ocean cluster which would ultimately skew the cloud temperatures. Using the approach in version 2 the cloudy-scene mean shifted to 1.6942 ppmv (σ =0.0866) and the surface temperature deviation similarly showed massive breakdown particularly at high cloud fractions where the

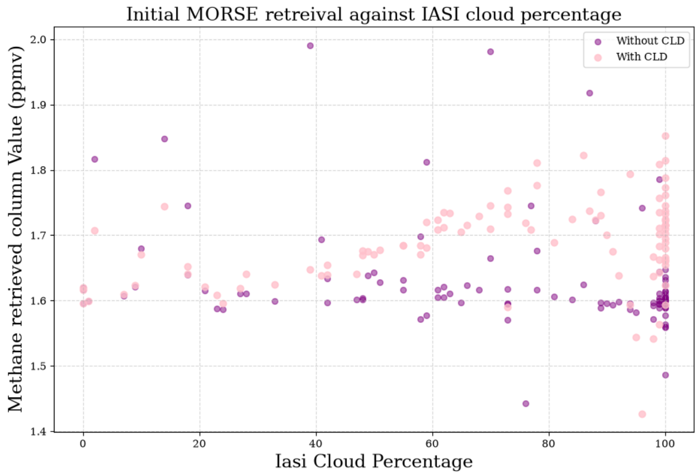

FIG. 9. Figure showing the retrieved methane column value as a function of IASI cloud percentage. The data for with and without the CLD flag enabled have been highlighted. The AVHRR data lead to an overall average increase in the methane column values.

mean deviation was -13.86 K. However, this stricter constraint caused retrieval failures to increase to 27. This likely artificially restricted the available radiometric and atmospheric data that MORSE had to work with. Hence, it likely lost flexibility in the iterative retrieval process, ostensibly leading to worsened retrievals.

The enforcement within version 3 attempted to ensure strict internal consistency between the geometric cloud fraction fed into the forward model and the derived radiative temperature. Ordering clusters by

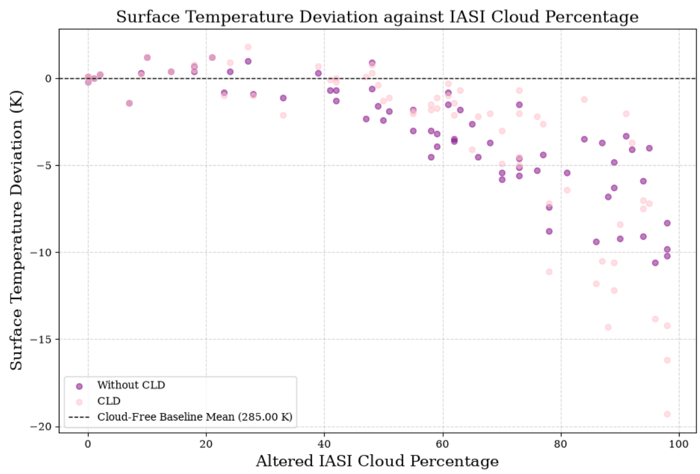

FIG. 10. Surface temperature deviations from the clear scene baseline (285 K) as a function of the reassigned IASI cloud percentage representative of the third version of MORSE considered.

warmth and explicitly reassigning the IASI cloud fraction to match the isolated cold cluster fraction yielded a cloudy mean of 1.6761 ppmv (σ=0.0788) with 20 failed retrievals. The version encouragingly showed the smallest deviation in the surface temperature at -3.58 K as shown in figure 10. At large values for the altered

IASI cloud percentage the surface temperature deviations reaches 10, 15, 20 degrees, which is a substantial improvement from many factors of hundreds of degrees for earlier versions.

VI. DISCUSSION

The values attributed to each version of MORSE highlight the delicate challenges of integrating high resolution AVHRR imager data into a coarse resolution IASI trace gas retrieval framework. A central insight emerging from Section IV is that the fraction of AVHRR pixels falling into the coldest cluster failed to correlate reliably with the official IASI cloud percentage. As demonstrated by removing homogeneous scenes and evaluating solar zenith angles, this disparity is not merely an artifact of daytime thermal contrast or simple scene uniformity. Instead, it underlines that sub-pixel cloud distributions are inherently complex, rendering binary cloud-clear approximations unlikely to be sufficient for accurate atmospheric modelling.

The underlying mismatch directly propagated into the methane retrievals evaluated in Section V, illustrating an intricate balance between physical consistency and algorithmic stability. If the cluster treatment worked as expected, the final retrieved values for Methane and Surface Temperature in cloudy scenes should match successfully to the values obtained from pristine cloud-free scenes. Across all tested MORSE configurations, cloud free pixels consistently anchored the dataset to a stable baseline mean (1.6107 ppmv, σ =0.0105), reflecting high measurement precision under pristine conditions. However, introducing cloud flags and refined temperature weightings into cloudy scenes induced notable shifts in both the retrieved methane and surface temperature values as well as the data scatter.

TABLE I. Summary of Retrieval Performance metrics across the MORSE versions

Statistics	V1	V2	V3
Avg Methane bias /ppmv	0.074	0.083	0.065
Methane std deviation /ppmv	0.069	0.086	0.078
Failed Retrievals	23	27	20
χ^2	9.41	10.22	5.14
Avg Surface Temp bias /K	-22.65	-13.86	-3.58

The results summarised in table 1 show that reassigning the IASI cloud percentage in Version 3 produced the most reduced value for the mean methane deviation, that being the difference between the mean methane column value for cloudy and the clear scenes. Version 3 also produced the lowest Chi-Squared value suggesting the MORSE forward model prediction more accurately matched the observed data. The first two versions suffered from server surface temperature bias, which was also greatly reduced in version 3 suggesting a significant improvement in the physical realism of the forward model.

VII. CONCLUSION

The project aimed to evaluate how AVHRR data can provide auxiliary information to help characterise cloud properties within the IASI footprint, which feeds directly into the radiative transfer forward models used to retrieve atmospheric trace gases like methane. There were modest improvements made to the retrieved mean methane column values, and the retrieved surface temperature bias was significantly reduced. This reflected the fact that the changes made improved the physical realism of the MORSE algorithm. Notwithstanding the improvements, the disparities between the cloud and cloud-free scenes were still substantial. The results underscore that clouds are very complex and its not entirely possible to achieve a fully satisfactory result for methane retrievals using just AVHRR data to model them. Future work may focus on multi-instrument synergies or adaptive cluster thresholds to better handle the intricate sub-pixel structures. The deployment of the IASI-NG instrument on the Metop-SGA1 satellite launched in 2025 [7] will likely continue to enhance atmospheric measurement precision. Even with next generation instrumentation, refined sub-footprint cloud treatments will remain essential for fully realizing the potential of trace gas retrievals in cloudy atmospheres.

VIII. APPENDIX

The conversion from spectral radiance to brightness temperature relies on Planck's Law of black-body radiation, which describes the electromagnetic spectrum emitted by a body in thermal equilibrium. Equations 3 and 4 show the equations used to convert to brightness temperature,

$$T_b = \frac{c_2}{\lambda \ln\left(1 + \frac{c_1}{\lambda^5 L_\lambda}\right)} \tag{3}$$

$$T_b = \frac{c_2 \tilde{\nu}}{\ln\left(1 + \frac{c_1 \tilde{\nu}^3}{L_{\tilde{\nu}}}\right)} \tag{4}$$

Where λ is the central wavelength, $\bar{\nu}$ is the central wavenumber, and L_λ (or $L_{\bar{\nu}}$) represents the observed spectral radiance. Furthermore, c_1 and c_2 are the first and second radiation constants, equal to $3.74177 \times 10^{-16}\,\mathrm{W}\cdot\mathrm{m}^2$ and $0.014388\,\mathrm{m}\cdot\mathrm{K}$ ($14388\,\mu\mathrm{m}\cdot\mathrm{K}$) respectively.

IX. REFERENCES

[1] Gallaher, D., Campbell, G., Meier, W., Moses, J. & Wingo, D. The process of bringing dark data to light: The rescue of the early nimbus satellite data. *GeoResJ* **6**, 124–134 (2015). URL https://www.sciencedirect.com/science/article/pii/S2214242815000212. Rescuing Legacy Data for Future Science.

[2] Clerbaux, C. *et al.* Tracking pollutants from space: Eight years of iasi satellite observation. *Comptes Rendus Geoscience* **347**, 134–144 (2015). URL https://www.sciencedirect.com/science/article/pii/S1631071315000590.

[3] Smith, N. & Barnet, C. D. Practical implications of climcaps cloud clearing and derived quality metrics. *Earth and Space Science* **10**, e2023EA002913 (2023). E2023EA002913.

[4] Earth Observation Data Group. MORSE. URL https://eodg.atm.ox.ac.uk/MORSE/. Accessed 2026-08-14.

[5] Moseman, A. & Trancik, J. Why do we compare methane to carbon dioxide over a 100-year timeframe? are we underrating the importance of methane emissions? MIT Climate Portal (2025). URL https://climate.mit.edu/ask-mit/why-do-we-compare-methane-carbon-dioxide-over-100-year-timeframe-are-we-underrating. Updated August 8, 2025.

[6] Sha, M. K. *et al.* Validation of methane and carbon monoxide from sentinel-5 precursor using tccon and ndacc-irwg stations. *Atmospheric Measurement Techniques* **14**, 6249–6304 (2021). URL https://amt.copernicus.org/articles/14/6249/2021/.

[7] EUMETSAT. The iasi-ng instrument (infrared atmospheric sounding interferometer-new generation) flying on the metop-sga1 weather satellite has sent back its first data. https://www.eumetsat.int/iasi-ng-instrument-metop-sga1-satellite-sends-back-first-data (2025). Accessed: August 2026.